JCTC Journal of Chemical Theory and Computation

Reaction of H_2 with a Binuclear Zirconium Dinitrogen Complex − Evaluation of Theoretical Models and Hybrid Approaches

Brian F. Yates,*,† Harold Basch,‡ Djamaladdin G. Musaev,§ and Keiji Morokuma*,§

School of Chemistry, University of Tasmania, Private Bag 75, Hobart TAS 7001, Australia, Department of Chemistry, Bar Ilan University, Ramat Gan, Israel, and Cherry L Emerson Center for Scientific Computation and Department of Chemistry, Emory University, Atlanta, Georgia 30322

Received December 12, 2005

Abstract: Molecular orbital and hybrid ONIOM (both IMOMO and IMOMM) calculations have been carried out on the important reaction of H_2 with a binuclear zirconium dinitrogen complex to test the efficacy of several structural models of the ancillary ligand. The complete experimental ligand, $PhP(CH_2SiMe_2NSiMe_2CH_2)_2PPh$, in the zirconium complex has been treated at the IMOMM level, while two smaller approximations of the ligand, $HP(CH_2SiH_2NSiH_2CH_2)_2PH$ and $(PH_3)_2(NH_2)_2$, have received the full molecular orbital treatment. The mechanism of dihydrogen addition has been compared with our earlier study (Basch, Musaev, and Morokuma *J. Am. Chem. Soc.* **1999**, *121*, 5754−5761). We find that the substituent effects do cause some small changes in both the structures of the complexes studied and the activation energies of the transition structures. However for the most part the potential energy profiles are very similar to our earlier study and lend support to our use of simple theoretical models to represent moderately large experimental structures.

Introduction

The study of the activation of the N≡N triple bond in the dinitrogen molecule and its subsequent chemical reactions has remained a productive area of research over quite a number of years.[1−66] On one hand there is interest in understanding the biological mechanism of nitrogen fixation, while on the other the practical goal is to develop a catalytic cycle to enable nitrogen reduction to be carried out under mild conditions. Tuczek and Lehnert have stated that the most promising catalytic cycles are those "based on the mono- and binuclear transition metal N_2 compounds that give NH_3 or N_2H_4 upon protonation".[23] The first report of the addition of H_2 to a metal-coordinated N_2 was made by Fryzuk and co-workers.[15] In these experiments it was shown that the dihydrogen molecule added to the binuclear metal dinitrogen complex $[P_2N_2]Zr(\mu\text{-}\eta^2\text{-}N_2)\text{-}Zr[P_2N_2]$, where $P_2N_2 = PhP(CH_2SiMe_2NSiMe_2CH_2)_2PPh$. This complex contains a coordinated N_2 molecule in a side-on bridging arrangement. It reacts with H_2 to produce a new complex having bridging Zr···H···Zr and N−H bonds where the original H−H bond is broken while the N−N bond is conserved.

Using theoretical techniques and a model complex **1**, $[p_2n_2]\text{-}Zr(\mu\text{-}\eta^2\text{-}N_2)Zr[p_2n_2]$, where $p_2n_2 = (PH_3)_2(NH_2)_2$, we showed previously[24,25] that the mechanism for this reaction proceeds in two steps (see Figure 1): (i) the activation of the H−H bond via transition structure **2** to form the intermediate diazenidohydride complex $[p_2n_2]Zr(\mu\text{-}\eta^2\text{-}N_2H)Zr[p_2n_2](\mu\text{-H})$, **3**, and (ii) migration of the Zr-bonded hydride ligand to a position bridging the two Zr atoms to form the diazenido-μ-hydride complex $[p_2n_2]Zr(\mu\text{-}\eta^2\text{-NNH})Zr[p_2n_2](\mu\text{-H})$, **7**. The entire reaction was calculated to be exothermic by 13−15 kcal mol^{-1} with an activation energy of 21 kcal mol^{-1}. Although not observed experimentally, our theoretical studies also indicated that there are two further low-energy structures on the potential energy surface, $[p_2n_2]Zr(\mu\text{-}NNH_2)Zr[p_2n_2]$,

* Corresponding author fax: +61 3 6226−2858; e-mail: Brian.Yates@utas.edu.au.
† University of Tasmania.
‡ Bar Ilan University.
§ Emory University.

10.1021/ct050320e CCC: $33.50
Published on Web 07/04/2006

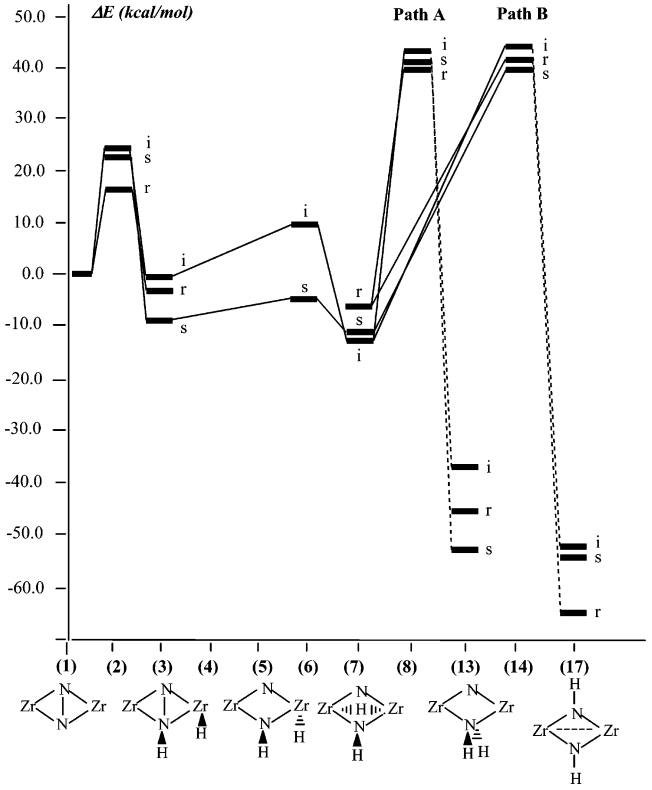

Figure 1. Potential energy surfaces calculated with the "c" (Zr−P constrained small model, s), "g" (intermediate model, i), and "j" (real system, r) levels of theory (see Tables 1 and 6). The dashed lines indicate that there are several intermediate minima and transition structures omitted between **8** and **13** and between **14** and **17**.

13, with a bridging NH_2, and $[p_2n_2]Zr(\mu\text{-}NHNH)Zr[p_2n_2]$, **17**, with two bridging NH units. These are about 40 kcal mol^{-1} more stable than **7** but are separated by barriers of nearly 60 kcal mol^{-1}.

The representation of the experimental macrocyclic $[P_2N_2]$ ligand by $(PH_3)_2(NH_2)_2$ is clearly a drastic approximation and one that we have been concerned to explore more fully. In our earlier work we noted that we could not use a more realistic representation of the ligand "because this would put the size of the calculations beyond current capabilities".[25] Although we have come a long way since the early calculations on bare Zr_2N_2 systems,[67] the straightforward molecular orbital calculation of the full experimental system still remains a difficult challenge for present-day computer facilities. Nevertheless, given the importance of the nitrogen fixation reaction and the current high level of interest in the activation of N_2 and other multiply bonded systems by organometallic complexes, it is important to assess the steric and electronic effects arising from the experimental $[P_2N_2]$ ligand. One of the difficulties we found in our earlier work with the model ligand was that one of the PH_3 ligands tended to escape from the first coordination shell to reduce the strain from overcrowding at the metal center. This produced unrealistically long Zr−P distances. These distances would not be possible in the chelated ligand, and to counteract this we fixed the Zr−P distance at 2.80 Å. We noted at the time that this was an oversimplification and that "it is highly desirable to reexamine the present results by using the real ligand".[25] Fryzuk and co-workers[68] have also carried out calculations using $(PH_3)_2(NH_2)_2$ as a model for the experimental $[P_2N_2]$ ligand in some tantalum complexes. They constrained several angles and a dihedral angle in an attempt to simulate the twist in the $[P_2N_2]$ ligand. However we must remember that the experimental ligand not only includes a structurally rigid aspect but also the steric and electronic factors arising from the phenyl groups on the phosphines.

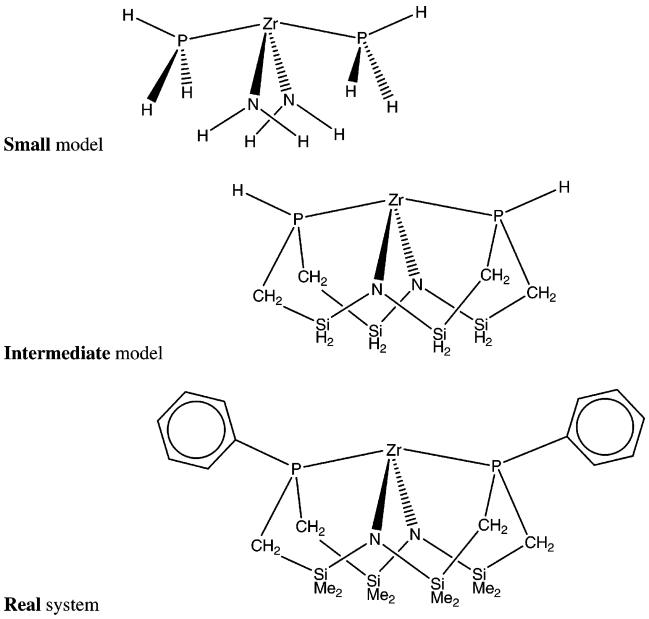

Figure 2. Definition of the different structural models used in this work.

One approach to using a more realistic ligand in the theoretical calculations is to use a larger model structure in the molecular orbital calculations. One might put substituents on the phosphorus or nitrogen to form, for example, $(PMe_3)_2(NMe_2)_2$, or one might include the basic skeleton of the macrocyclic ring, P(C−Si−N−Si−C)$_2$P, with just hydrogen substituents. Another approach is to use a hybrid theoretical technique such as the ONIOM method[69,70] which allows the complete experimental system to be included at least at a low level of theory (such as semiempirical MO or molecular mechanics), while a high level of molecular orbital theory is retained for the most important part, the reaction center.

In this paper we report our theoretical studies using both approaches. We have used a larger model for the experimental ligand in the MO calculations, and we have combined this with both IMOMO and IMOMM hybrid theoretical treatments. We have re-evaluated the reaction mechanism for complexes **1**−**7** corresponding to the experimentally observed process and in addition have recalculated the key structures (**8**, **13**, **14**, **17**) on the remainder of the potential energy surface.

Theoretical Methods

As stated in the Introduction, we have used a number of different structural models to represent the macrocyclic P_2N_2 ligand (see Figure 2). The model that we used in our original work,[25] ($(PH_3)_2(NH_2)_2$), we will refer to here as the "small model". The "intermediate model" incorporates the basic macrocyclic skeleton ($PH(CH_2SiH_2NSiH_2CH_2)_2PH$) without

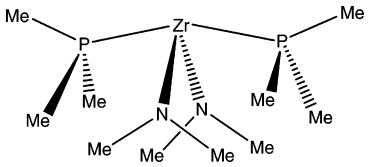

Figure 3. Alternative intermediate model.

the steric bulk of the extra methyl and phenyl groups. The third model structure used in this study corresponds to the real experimental system. These three structural models also correspond to the different layers that we have used in the hybrid theoretical methods discussed below.

In our molecular orbital calculations we have used several different basis sets. We began with the minimal LANL2MB basis set which incorporates the Hay and Wadt[71] small-core relativistic effective core potential and minimal valence basis set on all atoms. This resulted in 94 basis functions (bf) for the small model systems and 182 bf for the intermediate model systems. We also used the "SBK" basis set which incorporates the SKBJ small-core relativistic effective core potential[72,73] together with the standard double-ζ basis set on Zr, CEP-31G on N, P, and Cl, and CEP-4G on H, C, and Si. That is, a double-ζ basis set is used on the atoms directly bound to Zr and a minimal basis set on the other atoms. In addition, diffuse functions (with Gaussian exponent of 0.04395) were included on Cl in the monomer and d-type polarization functions (with Gaussian exponent of 0.8) on the bridging N_2 in structures **1**−**17**. In the separate calculations on the small model systems (i.e. the nonhybrid method), the CEP-31G basis set was used on hydrogen instead of CEP-4G. The SBK basis set combination as defined here resulted in 174 bf for the small model systems and 254 bf for the intermediate model systems. The small model systems were reoptimized with a slightly larger basis set (SBKBS1) in which polarization functions were added to all atoms connected to zirconium (CEP-31G* was used for N, P, and

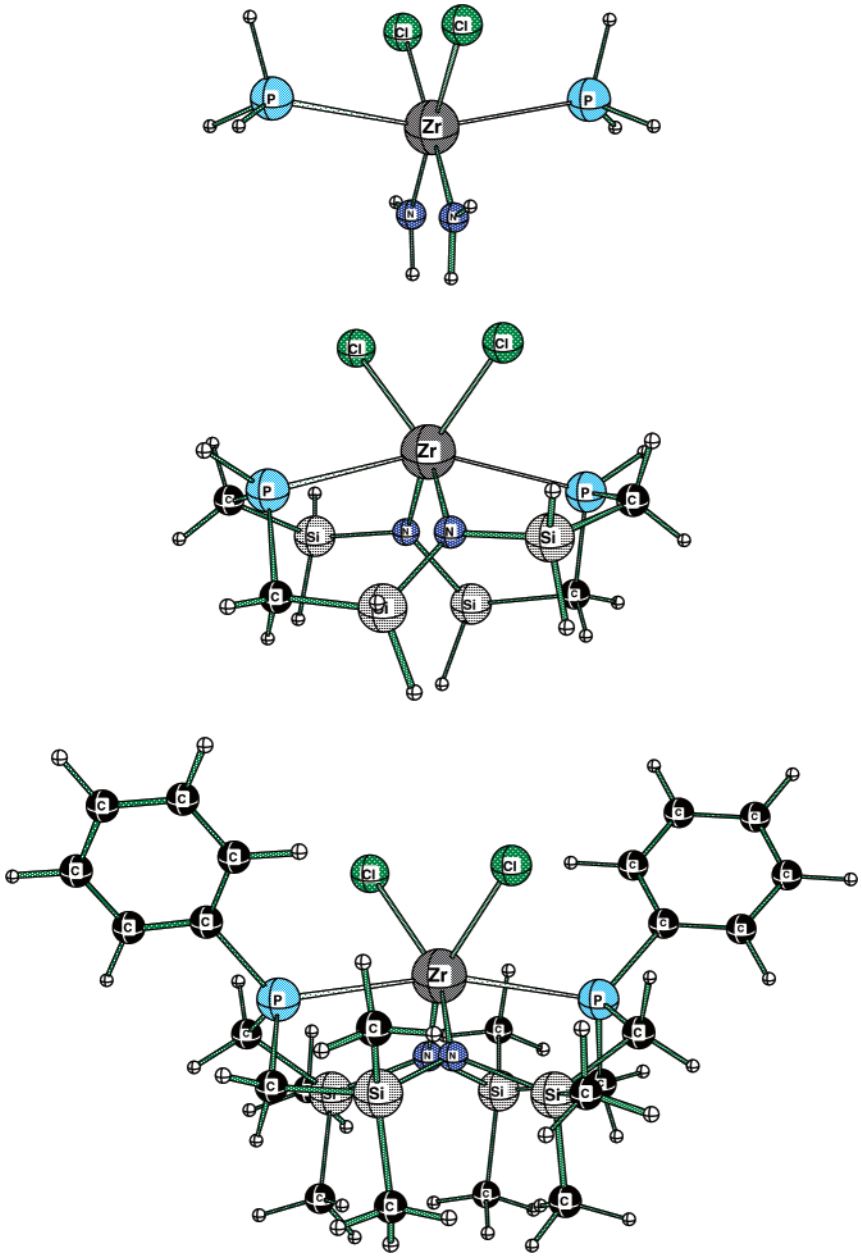

Figure 4. Monomer (small, intermediate, and real systems).

Table 1. Theoretical Methods Used in This Work[a]

structural model	theoretical method	
small model	a	B3LYP/SBK
	b	B3LYP/SBKBS1
	c	B3LYP/SBKBS2//"b"
intermediate model	d	RHF/LANL2MB
	e	IMOMO(B3LYP/SBK small:RHF/LANL2MB intermediate)
	f	B3LYP/SBK
	g	B3LYP/SBKBS2//"f"
real system	h	IMOMM(RHF/LANL2MB intermediate:UFF real)
	i	IMOMM(B3LYP/SBK intermediate:UFF real)
	j	B3LYP/SBKBS2//"i"

[a] All structures were optimized at each level of theory, except for "c", "g", and "j" which represent single point calculations on geometries from "b", "f", and "i", respectively.

Cl). Finally single point calculations were carried out on all systems (small, intermediate, and real) using a more flexible basis set (SBKBS2) which was valence-triple-ζ on zirconium, valence-triple-ζ plus polarization and diffuse functions on all atoms connected to zirconium, and valence-double-ζ plus polarization functions on all remaining atoms. This last basis set resulted in 333 bf for the small model, 572 bf for the intermediate model, and 1188 bf for the real system. Full details of the basis sets used are given in the Supporting Information.

RHF and density functional (B3LYP[74−76]) calculations were carried out at the molecular orbital level of theory. The initial SCF convergence in nearly all of the systems was problematic and required the judicious use of saved molecular orbital coefficients and level shifting. In some cases we employed stability tests[77,78] followed by reoptimization of the wave function (the "stable = (opt,rrhf)" keyword was used in the Gaussian program) to ensure that the correct wave function was used. Full geometry optimizations were carried out together with vibrational frequency calculations. Transition structures were characterized by the determination of only one imaginary frequency and by slightly distorting along the imaginary frequency normal mode in both directions and performing geometry minimizations using the transition structure force constants as the initial Hessian.

A number of hybrid theoretical methods was used. In this approach the most important part (reactive region) of the system is treated with a high level of theory, while the less important parts are treated with a low level of theory. The ONIOM method[69,70] was used to carry out IMOMO and IMOMM calculations on the intermediate and real model systems. In the IMOMO calculations we used B3LYP/SBK for the core region (small model, layer 1) and RHF/LANL2MB for the outer region (intermediate model, layer 2). In the IMOMM calculations[79−82] we defined the intermediate model as the core region (layer 1) and the remainder of the real system as layer 2. We used either RHF/LANL2MB or B3LYP/SBK to treat layer 1 and the UFF[83] or MM3[84,85] force fields for layer 2. In the MM3 calculations, the UFF van der Waals parameters by Rappé et al. were used for the Zr atoms,[83] while all other MM contributions

Table 2. Comparison of Selected Calculated Values with Experiment for Monomer

	model							
	small		intermediate			real		
	a[a]	b[a]	d[a]	e[a]	f[a]	h[a]	i[a]	X-ray[b]
Zr−N1	2.063	2.077	2.038	2.211	2.122	2.096	2.179	2.136(4)
Zr−N2	2.063	2.077	2.038	2.211	2.122	2.096	2.179	2.125(4)
Zr−P1	2.847	2.842	2.875	2.738	2.823	2.768	2.704	2.694(2)
Zr−P2	2.847	2.842	2.875	2.738	2.823	2.768	2.704	2.707(2)
Zr−Cl1	2.571	2.532	2.573	2.519	2.538	2.578	2.539	2.455(2)
Zr−Cl2	2.571	2.532	2.573	2.519	2.538	2.577	2.539	2.448(2)
N−Zr−N	86.6	85.5	95.1	104.0	92.8	104.2	105.8	96.8(2)
P−Zr−P	160.5	161.3	152.8	144.2	156.5	154.0	152.0	152.25(6)
Cl−Zr−Cl	98.1	98.8	91.1	87.2	91.1	89.0	89.0	82.57(7)
N1−Zr−Cl2	87.7	87.9	90.6	89.7	93.9	89.2	88.0	89.5(1)
N2−Zr−Cl1	87.7	87.9	90.6	89.7	93.9	89.2	88.0	91.3(1)

[a] Level of theory, see Table 1. [b] Fryzuk et al. *Organometallics* **1998**, *17*, 846−853. Atom numbering scheme in Figure 1 of that paper is used in the table above.

Table 3. Comparison of Selected Calculated Values with Experiment for Structure 1

	model							
	small		intermediate			real		
	a[a]	b[a]	d[a]	e[a]	f[a]	h[a]	i[a]	X-ray[b]
Zr1−N1	2.106	2.100	2.005	2.055	2.057	2.018	2.070	2.010(2)
Zr1−N3	2.116	2.121	2.118	2.251	2.171	2.166	2.209	2.203(4)
Zr1−P1	2.943	2.907	2.996	2.774	2.821	2.797	2.784	2.724(2)
N1−N2	1.530	1.518	1.507	1.539	1.508	1.498	1.506	1.43(1)
N3−Zr1−N4	118.9	117.1	116.4	119.0	114.3	112.4	110.4	108.4(2)
P1−Zr1−P2	159.6	161.0	137.6	139.2	142.0	134.6	136.2	140.90(7)
N1−Zr1−N2	43.2	42.7	44.0	44.0	42.9	43.3	42.4	41.8(3)
Zr1−N1−N2	70.3	67.3	68.3	67.9	68.9	69.0	69.7	69.1(2)
N1−N2−Zr1−Zr2	−46.8	−45.7	−17.1	−36.8	−44.2	−13.3	−15.0	

[a] Level of theory, see Table 1. [b] Fryzuk et al. *Science* **1997**, *275*, 1445−1447.

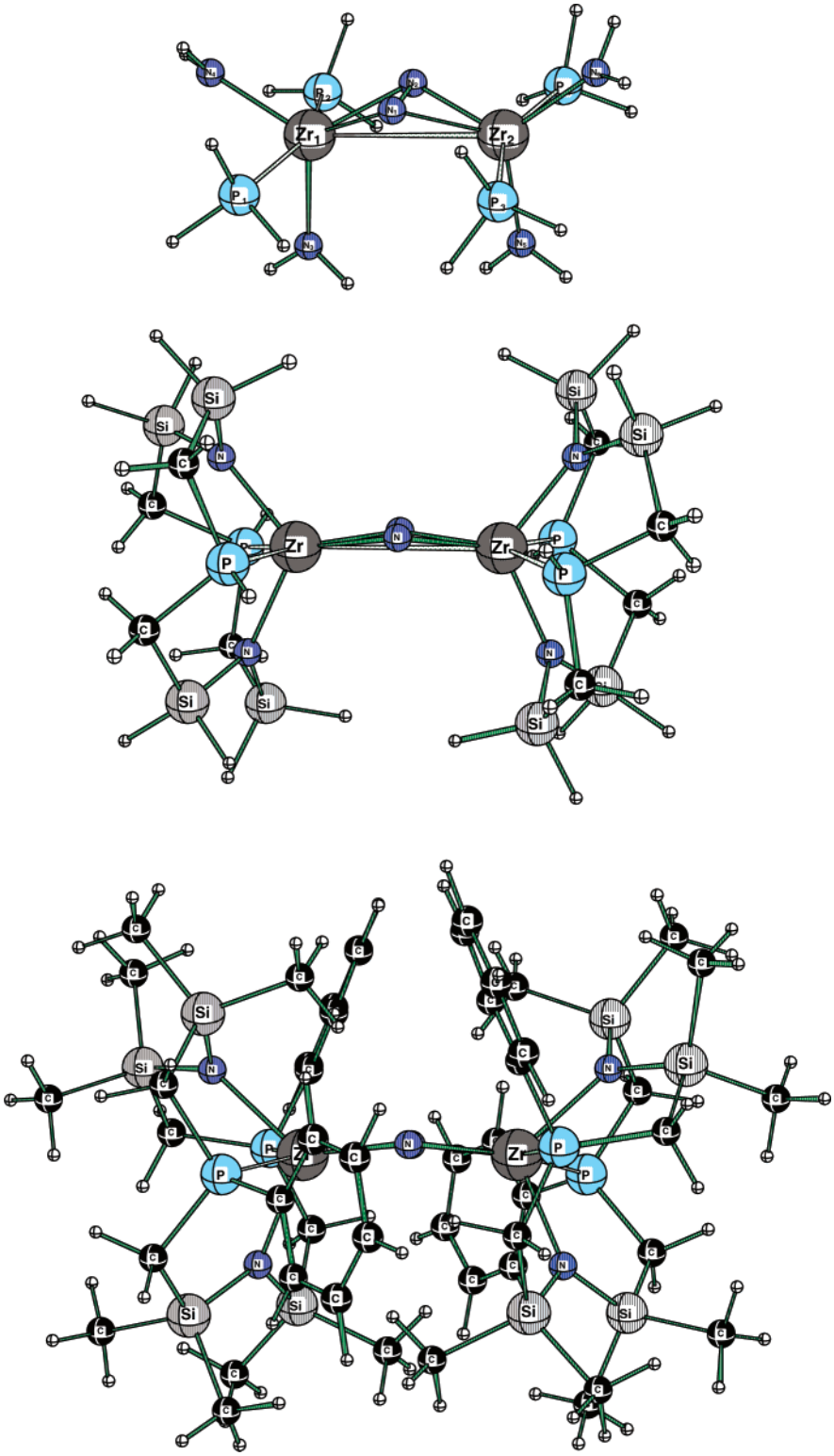

Figure 5. Structure **1** (reactant) (small, intermediate, and real systems).

involving the metal atoms were set to zero. The IMOMM link bonds were fixed at R(P−H) = 1.435 Å and R(Si−H) = 1.490 Å.

In our initial IMOMM calculations we used the small model (Figure 2) for the MO calculations and the real system for the MM calculations. However this lead to the Si−C distance in the calculated real system becoming too large. The Si−C bond corresponds to the nonbonded H···H distance in the small model, and it turns out that this leads to the calculation of an unrealistic repulsion in the small model. Our initial attempts to use the alternative intermediate model shown in Figure 3 for the MO level also lead to

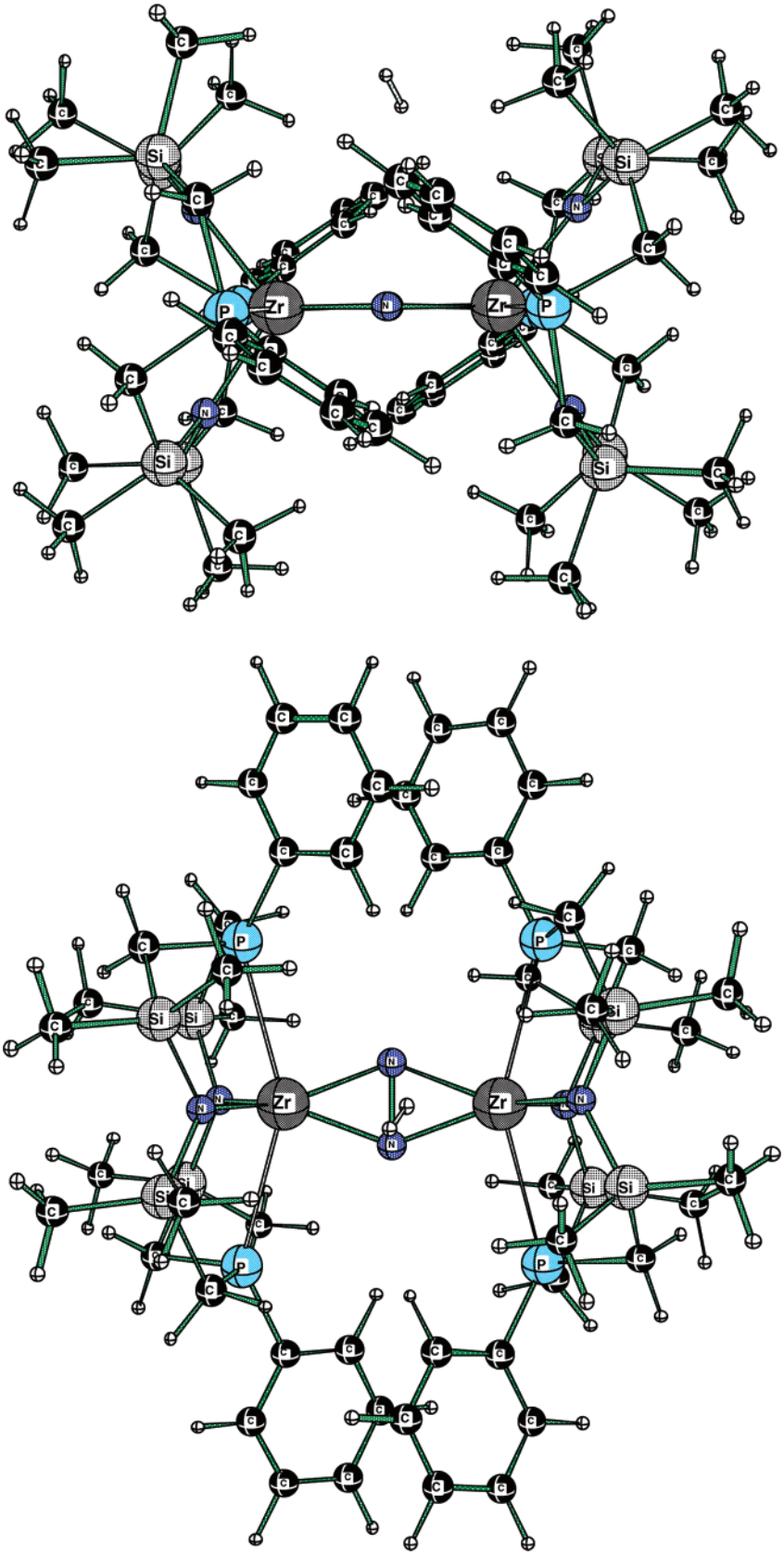

Figure 6. H_2 entering the coordination sphere: view from side-on (top) and from above (bottom).

unrealistic repulsions being calculated. Thus it is essential that the N−Si−C−P linkage be included in the MO portion of the calculation. We have studied this problem in detail previously for the *n*-butane system.[81]

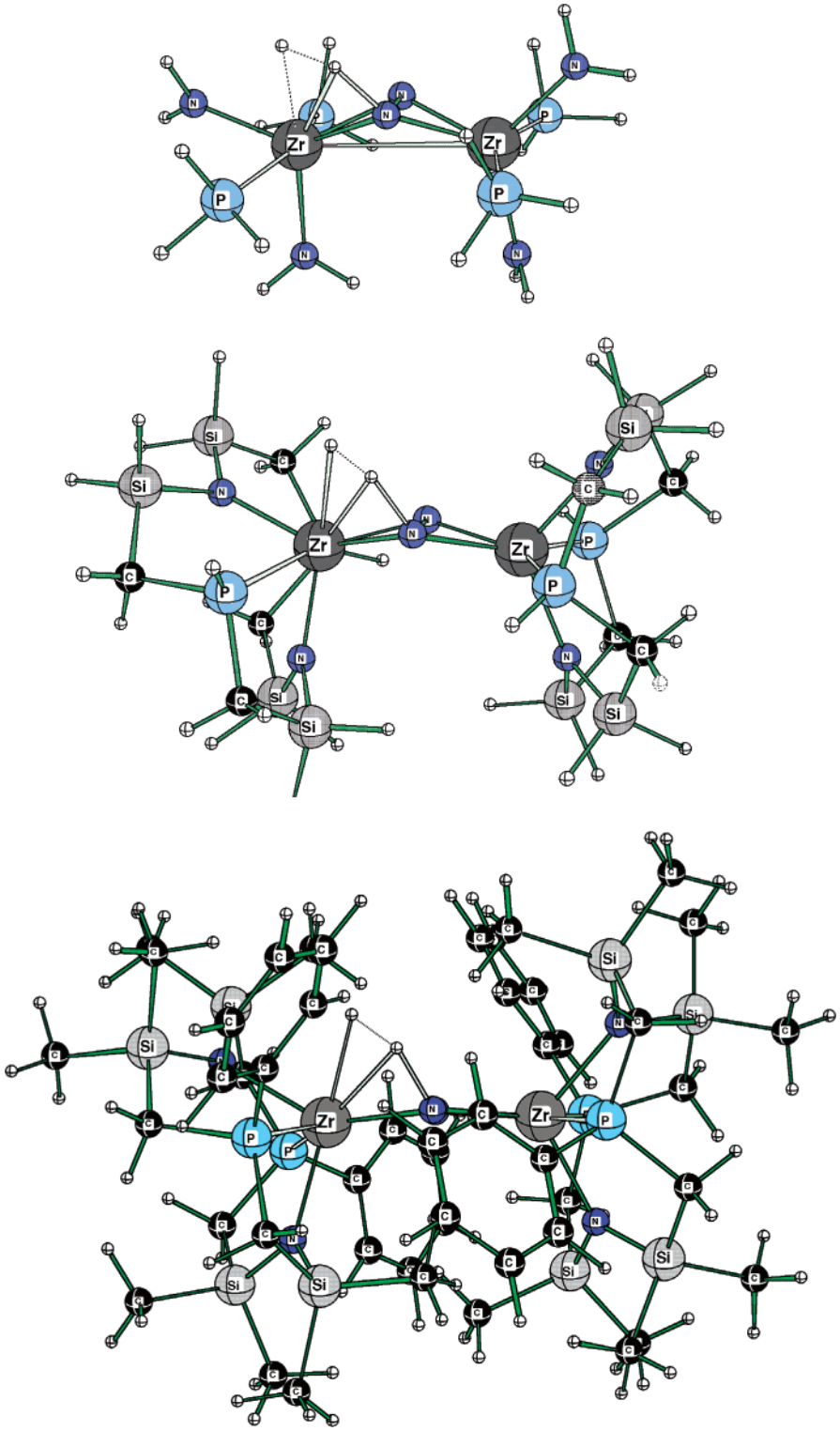

Figure 7. Structure **2** (TS) (small, intermediate, and real systems).

The theoretical methods used in this work are summarized in Table 1. This allows a number of comparisons to be made which assist in evaluating the theoretical approaches we have used and in separating out the different effects. In particular the effect of the level of theory can be assessed by comparing a with b (Table 1), d with f, e with f, and h with i. The effect of substituents can be assessed by comparing a with e, a with f, d with h, and f with i.

All calculations were carried out with the Gaussian 98[86] or Gaussian 03[87] programs, except for some IMOMM calculations which were performed with the IMOMM code[79] and the MM3(92)[84] and Gaussian92/DFT[88] programs.

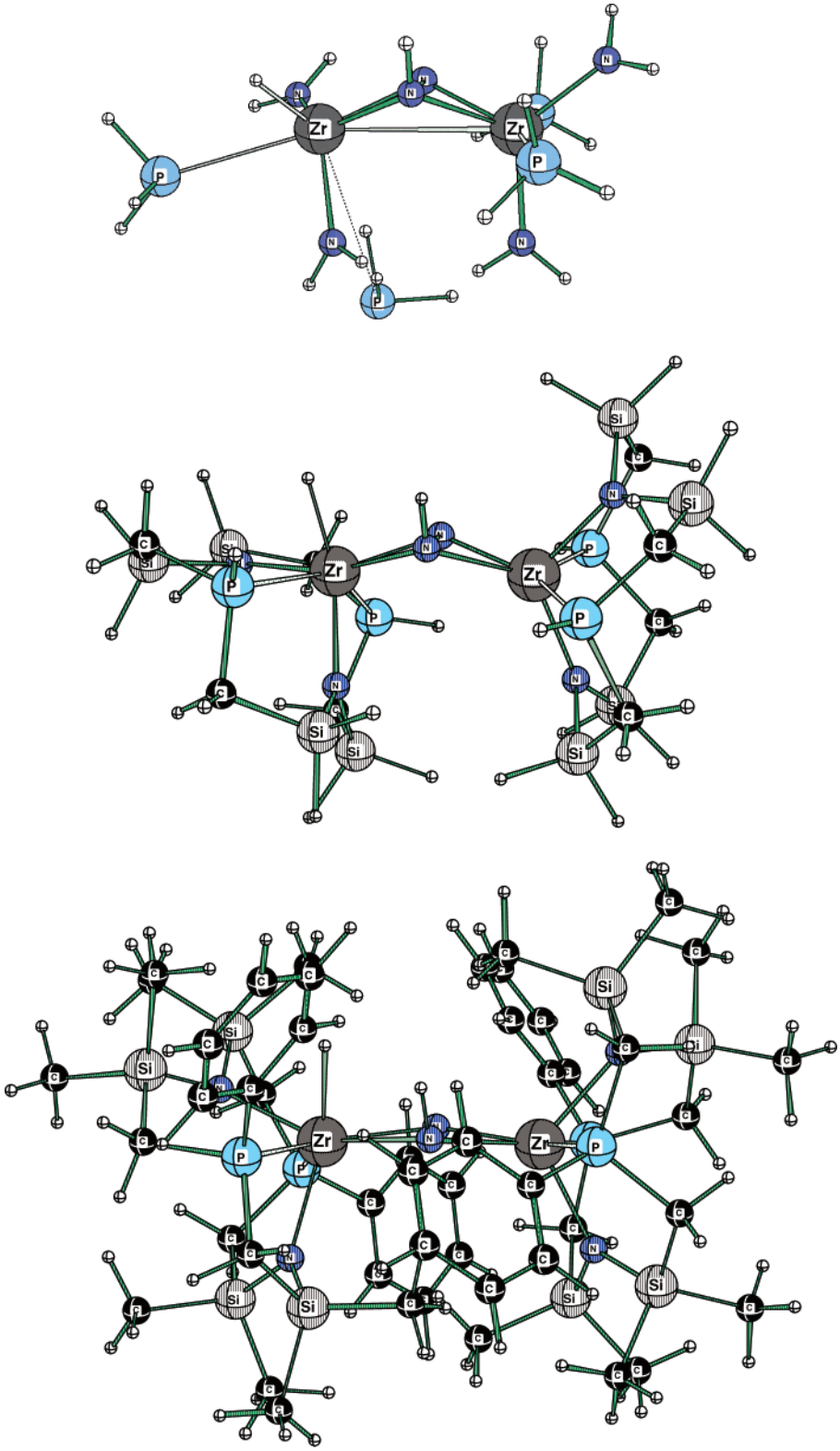

Figure 8. Structure **3** (small, intermediate, and real systems).

Results and Discussion

Geometries. Results are presented here for the monomer (one-half of the binuclear zirconium complex), the first part of the potential energy surface, **1**−**7**, and the key structures (**8**, **13**, **14**, **17**) on the remainder of the potential energy surface. In our previous work[25] we showed that **8** was connected to **13** (and **14** was connected to **17**) by a series of low-energy stationary points on the potential surface. These stationary points have not been considered in this work, but we have retained the same numbering system to allow comparison with our earlier study.

The structure of the monomer is shown in Figure 4 for the three model structures used in this work (small − intermediate − real, going from top to bottom). Table 2

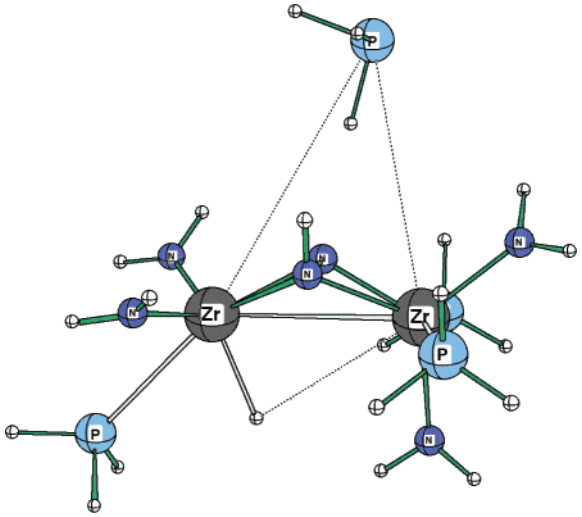

Figure 9. Structure **5** (small model).

includes values for the experimental geometry of the monomer as determined by X-ray analysis.[22] This shows that the N−Zr−N angles are calculated to be too small and the Cl−Zr−Cl angles too large in the small model. There is an improvement in these geometrical parameters on moving to the intermediate model. At the B3LYP/SBK level for the intermediate model (column f in Table 2) the calculated geometry agrees very well overall with the experimental geometry. On moving to the real system (column i) the Zr−P distances move even closer toward the experimental ones, accompanied by a slight opening of the N−Zr−N angle.

The structure of complex **1** is shown in Figure 5 for the three models used. It can be seen quite clearly that the Zr_2N_2 ring approaches planarity as one moves from the small model to the real system. This is shown more quantitatively in Table 3 where the dihedral angle for these four atoms is shown in the last row of the table. This is a significant result because we[25] and others have shown that the Zr_2N_2 core is strongly bent in model complexes, and a careful analysis of the electronic factors which give rise to the butterfly structure has recently been carried out.[50] The results presented here demonstrate that steric factors can overcome this electronic preference for bending and lead to a planar Zr_2N_2 core as the preferred geometry. What are these steric factors? When we noted in our earlier study[25] that the small model of **1** has a bent structure, we suggested that the extended macrocyclic ligand may prevent this bending. However it is clear from Table 3 that the basic skeleton of the macrocyclic ligand which is present in the intermediate model does not by itself confer planarity. In particular, a comparison of columns a and f shows that at the same level of theory the small and intermediate models are bent by nearly the same amount. Clearly the presence of the phenyl groups is required to achieve planarity.

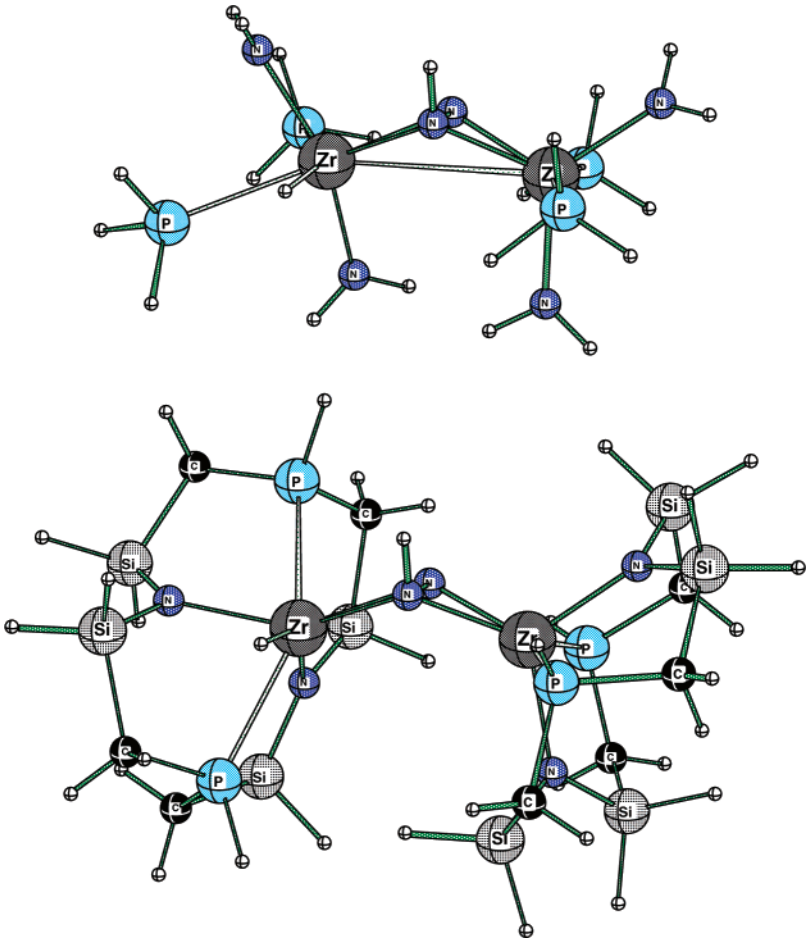

Figure 10. Structure **6** (small (constrained Zr−P) and intermediate models).

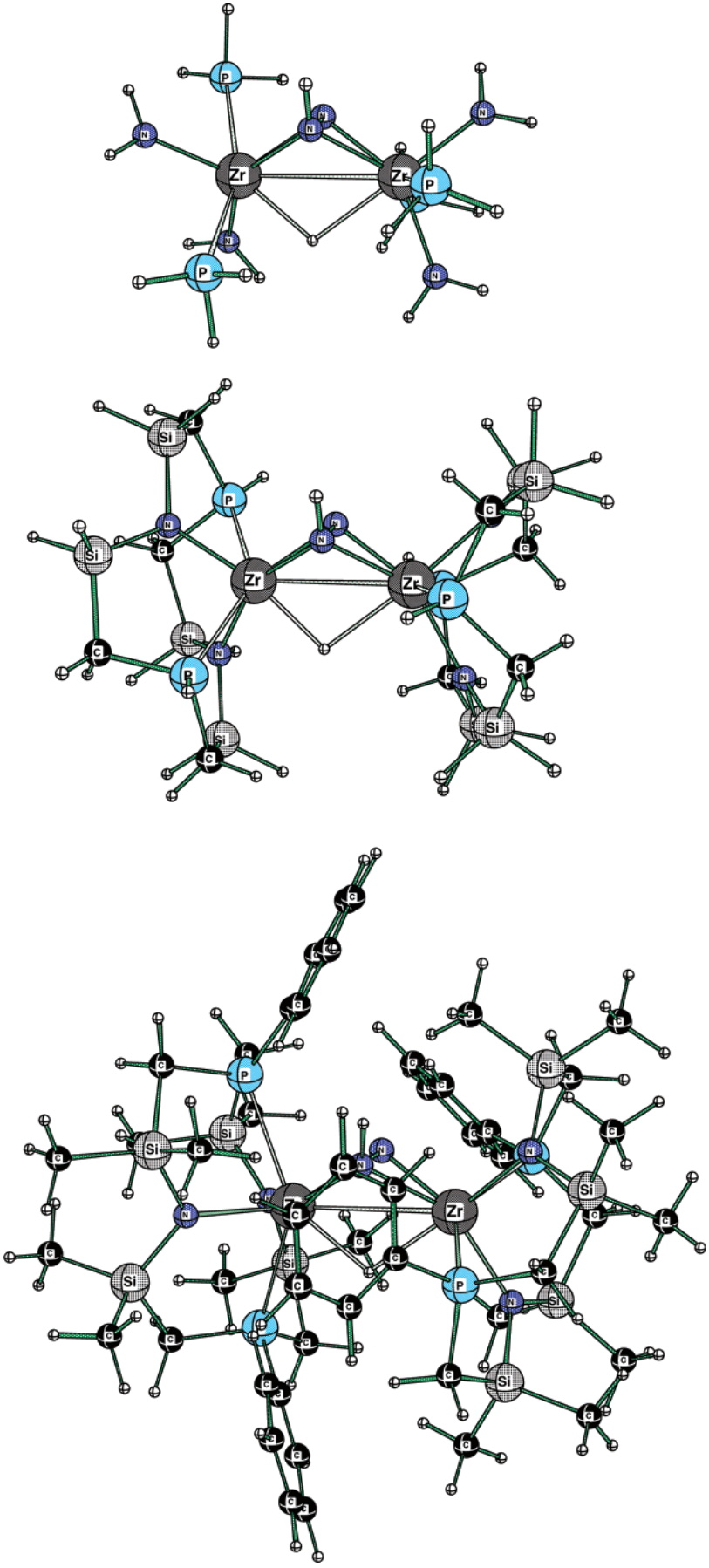

Figure 11. Structure **7** (small, intermediate, and real systems).

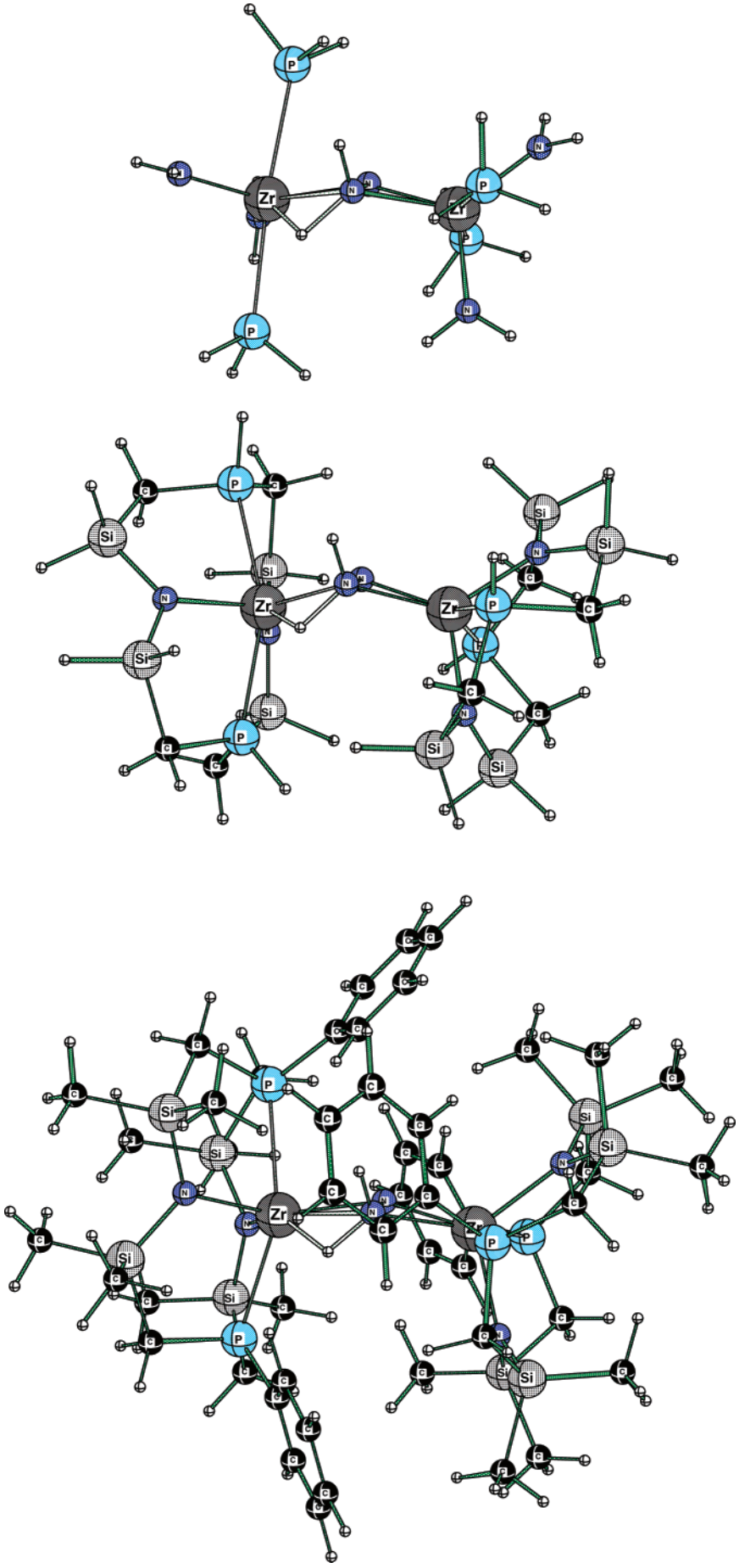

Figure 12. Structure **8** (small, intermediate, and real systems).

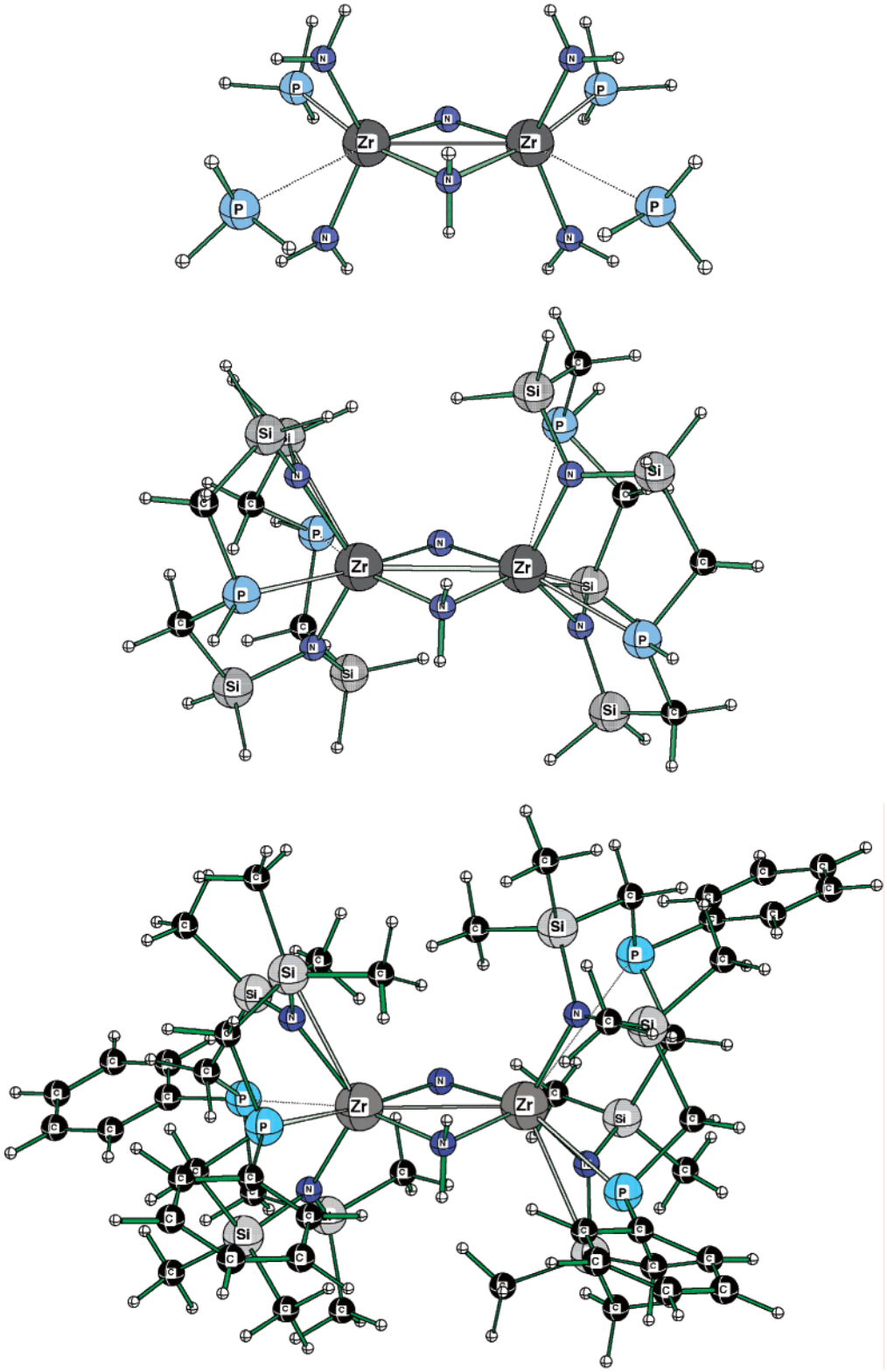

Figure 13. Structure **13** (small, intermediate, and real systems).

The experimental X-ray structure for **1** is also shown in Table 3.[15] This indicates that the Zr−P distances are once again overestimated in the small model and also at the RHF/LANL2MB level for the intermediate model (column d), but they are improved with the combination of the larger models and the B3LYP/SBK level of theory. Comparing columns a, f, and i it can be seen that the overestimation in the Zr−P distance decreases from 0.22 to 0.10 to 0.06 Å, respectively. The P−Zr−P angle is also overestimated with the small model but improves with the larger systems.

In Figure 6 we show a picture of the dihydrogen molecule entering the coordination sphere of the real system (this picture is obtained by minimization from transition structure **2** downhill toward the reactants). From the side-on perspective it appears that the H_2 would be prevented from reaching the nitrogens at the center of the complex by the shield of

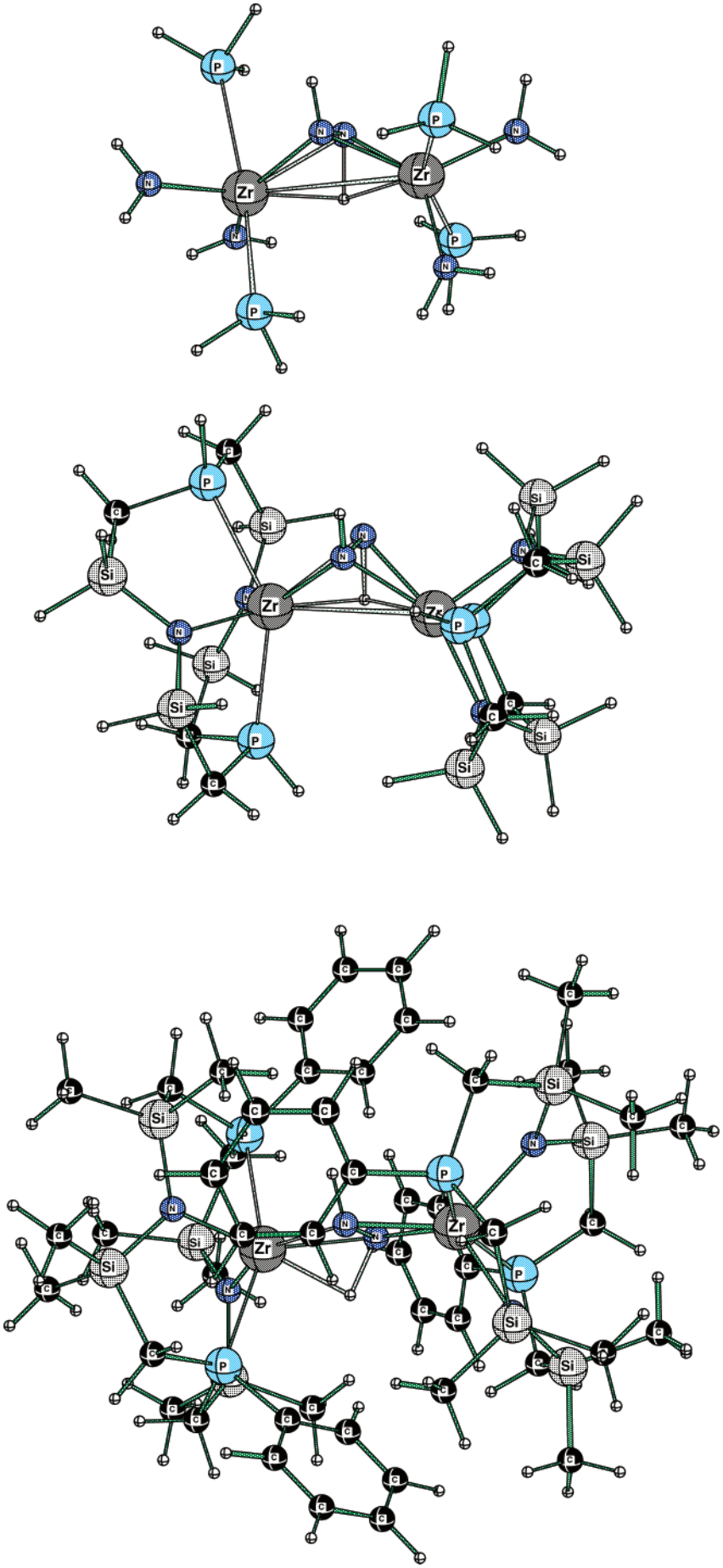

Figure 14. Structure **14** (small, intermediate, and real systems).

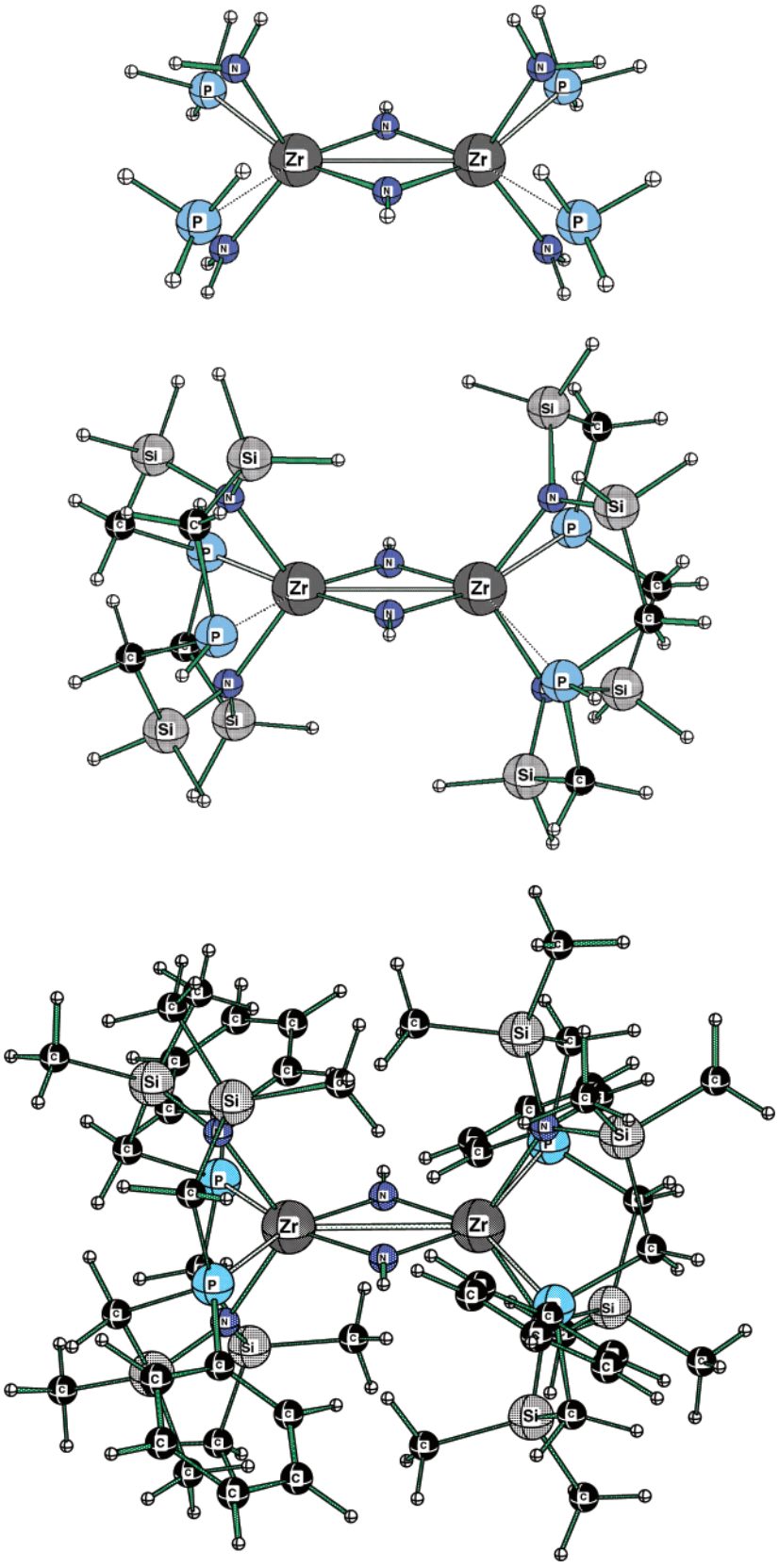

Figure 15. Structure **17** (small, intermediate, and real systems).

phenyl rings on the phosphines. But the view from above shows that phenyl rings are well clear of the reaction center and that the H_2 has a clear approach.

Figure 7 shows the actual transition structure for the coordination of the H_2. The key $Zr_2N_2H_2$ part of the geometry looks very similar for the three models used. The Zr−H

distances decrease on going from the small model to the real system by 0.1−0.2 Å (see Supporting Information) which might indicate slightly greater binding in the real system; however, the H−H, N−N, and N−H distances remain almost the same.

The first product from this reaction, **3**, is shown in Figure 8. Once again we note the unrealistic loss of a phosphine in the small model. As expected, the phosphine is not dissociated in the intermediate model or the real system, and there is no need to fix the Zr−P distance in order to obtain a reasonable geometry. There appears to be a general tendency toward planarity as one moves to the real system, but the N−N−Zr−Zr portion is by no means completely flat. At the "a", "f", and "i" levels of theory the calculated N−N−Zr−Zr dihedral angle is −57.8, −49.2, and −13.5°, respectively.

Figure 9 shows the structure of complex **5** with the small model. We noted previously[25] that this is an artifact of the unconstrained ligand system, and indeed no corresponding structure could be found in this work when the intermediate model or real system was employed.

After much computational effort in searching the potential energy surfaces, we were finally able to locate a transition structure **6** which connects structures **3** and **7** at the small (constrained Zr−P) and intermediate models. The geometry of **6** is shown in Figure 10. We were unable to locate **6** for the unconstrained Zr−P small model, which is consistent with the comments made in the previous paragraph. Clearly the potential energy surface for **3** → **7** is different for the constrained and unconstrained small model. At the "f" level of theory transition structure **6** was shown to have a single very small imaginary frequency of just 27*i* cm^{-1}. Nevertheless, by carefully distorting the structure along the normal mode corresponding to this imaginary frequency we were able to verify that it connected up with structure **3** in one direction and structure **7** in the other. Transition structures such as this with very small imaginary frequencies are quite difficult to locate, and although we explored several different possibilities for the real system, we were unable to find a suitable structure at that level within a reasonable expenditure of computer time.

The experimentally observed product, **7**, is shown in Figure 11. An extensive comparison of the calculated geometries with the experimental neutron diffraction data[24] is included in the Supporting Information. The average absolute deviations from experiment for the "a", "f", and "i" levels of theory are 0.13, 0.07, and 0.07 Å, respectively, for bond distances and 12, 8, and 4° for bond angles. There is improvement in the Zr−P distances and in most of the angles on going from the small model to either the intermediate model or the real system. Structure **7** is quite bent around the Zr_2N_2 portion at all levels of theory (in contrast to **1** and **3**) which is expected due to the bridging hydrogen. The N−N−Zr−Zr dihedral angle is 66−70° at all levels of theory. The bridging hydrogen is fairly equidistant from both zirconiums at all levels of theory, although not to the same extent as indicated by the neutron diffraction data (see Supporting Information).

Transition structure **8** is shown in Figure 12. It adopts an almost planar Zr_2N_2 geometry in the intermediate and real systems, and the Zr−P distances are all quite reasonable (<2.8 Å). Minimizations along the normal mode corresponding to the imaginary frequency showed that **8** connects **7** with **9** for the intermediate model and real system. (Structure **9** was not investigated further here, but its geometry and relative energy were consistent with the corresponding structure **9** that we previously studied for the small model.) Previously we showed that with the small model, transition structure **8** connects **5** with **9** (rather than **7** with **9**), but once again this is an artifact of the unconstrained phosphine ligands in the small model; when Zr−P is constrained to remain at 2.80 Å, then this transition structure connects **7** with **9** as expected. This represents a slight change to our earlier mechanism in that now we conclude that the experimentally observed structure **7** is the common starting point for pathway A and pathway B (Figure 1) (leading to further low-energy structures).

The optimized geometries for structure **13** are shown in Figure 13. The unconstrained geometry for the small model adopted very nearly C_2 symmetry, and so this symmetry constraint was imposed for the remaining optimizations. This was verified by frequency calculations at the "f" level of theory. The core of the molecule exhibited very little change on going from the small to the intermediate model to the real system, with the Zr_2N_2 portion being planar at all levels of theory. Two partially dissociated phosphines are retained in all cases. This is an interesting observation since it implies that in the real system the macrocyclic ligand has enough flexibility to allow some lability in coordination to the zirconium.

Transition structure **14** is shown in Figure 14. It has a rather bent structure in the small and intermediate models and a fairly short N−N distance for the bridging nitrogens (1.49 Å). Minimizations along the normal mode corresponding to the imaginary frequency showed that **14** connects **7** with **15** for the small, intermediate, and real systems. (Structure **15** was not investigated further for the intermediate and real systems.)

Figure 15 shows the structure of product **17**. As with structure **13**, an unconstrained geometry optimization on the small model suggested a C_2 symmetric structure, and this point group was imposed for the remaining optimizations and verified by frequency calculations at the "f" level of theory. With the small model, two of the phosphines are dissociated. In the intermediate model two slightly elongated Zr−P distances are retained although overall the structure looks quite reasonable. In the real system there are no unbound phosphine ligands, and all four Zr−P distances are perfectly acceptable. The Zr_2N_2 portion is shown to be almost planar at all levels of theory.

As discussed by Fryzuk[33,50,56] and others,[28,89] the degree of activation of N_2 is often measured by the increase in the N−N bond length and decrease in the N−N stretching frequency compared to molecular nitrogen. In Table 4 is shown the N−N bond lengths, stretching frequencies, and force constants calculated at the B3LYP/SBK level of theory for the intermediate model of all the structures in this study.

Table 4. N−N Bond Lengths, Vibrational Frequencies, and Force Constants for the Intermediate Model Structures Calculated with B3LYP/SBK[a]

structure	r_{N-N} (Å)	ν_{N-N} (cm^{-1})	f_{N-N} (mDyne/Å)
N_2	1.132	2445	49.33
1	1.508	795	3.03
2	1.523	722	0.84
3	1.505	834	0.86
6	1.499	859	1.43
7	1.482	872	1.86
8	1.494	846	1.29
13	2.808	480	0.76
14	1.485	854	0.94
17	2.656	645	0.95

[a] Fully optimized geometries from the "f" level of theory were used.

Much more sophisticated analyses have been carried out for similar model structures,[50,56] and the results in Table 4 represent a fairly simplistic treatment of the vibrational frequencies. Apart from the obvious activation in all the structures of N_2 compared to molecular nitrogen, this table shows that there is a remarkable similarity in the N−N stretching frequencies of structures **1**−**8**. At first sight this might suggest a similarity in the N−N bond strengths in these structures; however, the calculated force constants indicate that there is a subtle variation in the N−N bonds across the series.

Energies. The relative energies of the structures considered in the current study are shown in Table 5 at seven different levels of model/theory. For structure **2** it appears that the RHF/LANL2MB level of theory (columns d and h) leads to an overestimate of the activation energy. All of the activation energies calculated in the present work increase in a very systematic manner from "a" to "f" to "i" (22, 27, 35 for **2**, 55, 67, 71 for **8**, and 55, 62, 72 kcal mol^{-1} for **14**, respectively). The relative energy of **3** is fairly similar across the different levels of theory except for "i". Since the geometry looks fine and since stability tests of the wave function indicate that the calculated energy is indeed for the lowest electronic state at this geometry, it is difficult to explain this discrepancy. Note that constraining the Zr−P distance in the ligand system in the small model has a pronounced effect in this case. This is also true of structures **13** and **17**, while for the remainder of the compounds it appears that constraining the Zr−P distance has little effect on the relative energies. The relative energies of **7**, **8**, and **14** are fairly similar across all levels of theory. The results for **8** and **14** correspond to full geometry optimizations. However for the intermediate and real systems we initially carried out calculations in which we froze the geometry of the central core of atoms at the transition structure geometries determined in our previous study for the small model, and then the remainder of the ligand system was minimized. This led to the activation energies being overestimated by 30−40 kcal mol^{-1} (see Supporting Information) and indicates the importance of allowing the core geometry to also be relaxed in the real system. The relative energies of **13** and **17** are similar across all the models we have used, except for column h which appears to overestimate their stability.

The effect of changing the level of theory in our calculations can be more clearly assessed by comparing column a with b in Table 5, d with f, e with f, and h with i. In the first case the energies are almost identical indicating that extra polarization functions on N and P had little effect. In the second case the energies are fairly similar except for **2**, **3**, **13**, and **17**, indicating that electron correlation is important for these systems. In the third case (e with f) the comparisons are quite excellent, indicating that the ONIOM treatment is a very effective model for the full B3LYP calculation. In the final case (h with i) the energies vary inconsistently indicating a possible problem with the RHF/LANL2MB component of the ONIOM calculations.

The relative energies from the singe point calculations at the B3LYP/SBKBS2 level of theory are shown in Table 6. Overall the consistency between the three different models is quite excellent (particularly if one focuses on the Zr−P constrained values in parentheses for the small model). This lends confidence to our conclusions about the mechanism of the dihydrogen activation (noting that **7** is now shown to be common to both pathways A and B). There are only minor differences in the relative energies between the three models, and the potential energy surfaces for the small, intermediate, and real systems are compared in Figure 1. A comparison of Table 6 with Table 5 also shows that the single point calculations did not change greatly the relative energies of the small and intermediate models; however, there are larger changes apparent for the real system. This might indicate

Table 5. Relative Energies (kcal mol^{-1}) for Optimized Geometries

	model						
	small		intermediate		real		
	a[a,b]	b[a,b]	d[a]	e[a]	f[a]	h[a]	i[a]
1	0 (0)	0 (0)	0	0	0	0	0
2	21.6(21.5)	22.2 (22.2)	43.0	24.5	26.7	49.5	34.6
3	−13.6(−8.4)	−14.0 (−10.2)	−10.1	3.9	3.1	7.7	19.0
6[c]	(−5.0)	(−6.2)	9.5	12.6	14.0		
7	−13.1(−13.0)	−13.7 (−13.6)	−13.9	−16.6	−15.3	3.0	7.9
8	43.4(42.0)	40.8 (40.3)	47.7	49.4	52.3	56.1	63.3
13	−65.5(−54.2)	−65.5 (−54.0)	−65.4	−47.9	−42.1	−110.9	−79.1
14	42.6(41.6)	40.0 (39.5)	39.6	44.7	46.9	17.3	64.3
17	−64.2(−51.1)	−65.3 (−52.5)	−74.7	−47.8	−56.9	−122.0	−102.3

[a] Level of theory, see Table 1. [b] Numbers in parentheses are calculated with Zr−P frozen at 2.80 Å. [c] Structure **6** could not be located at some levels of theory—see text.

Table 6. Relative Energies (kcal mol^{-1}) for Single-Point Calculations

	model		
	small c[a,b]	intermediate g[a]	real j[a]
1	0 (0)	0	0
2	22.4(22.5)	24.3	16.3
3	−13.3(−9.2)	−0.7	−4.3
6	(−4.9)	9.6	
7	−12.5(−12.3)	−13.8	−7.2
8	41.1(40.5)	42.8	39.5
13	−66.3(−53.4)	−36.9	−44.6
14	40.1(39.6)	44.5	42.1
17	−68.3(−53.5)	−52.0	−64.2

[a] Level of theory, see Table 1. [b] Numbers in parentheses are calculated with Zr−P frozen at 2.80 Å.

Table 7. Substituent Values (kcal mol^{-1})[a,b]

structure	Subst(RHF/LANL2MB)	Subst(B3LYP/SBK)
1	0(0)	0(0)
2	11.8 (7.0)	5.1(5.2)
3	36.7 (36.7)	16.7(11.5)
6		(9.0)
7	30.6 (6.6)	−2.2 (−2.3)
8	70.2 (46.4)	8.9(10.3)
13	27.6 (−1.2)	23.4 (12.1)
14	66.6 (39.9)	4.3(5.3)
17	6.5 (−36.8)	7.3 (−5.8)

[a] Here, Subst(method) = Rel E (method//method)$_{intermediate}$ − Rel E (method//method)$_{small}$ e.g. Subst(B3LYP/SBK) = Rel E (B3LYP/SBK//B3LYP/SBK)$_{intermediate}$ − Rel E (B3LYP/SBK//B3LYP/SBK)$_{small}$ = "f" − "a". [b] Numbers in parentheses are calculated with Zr−P frozen at 2.80 Å.

the limitations of using the UFF force field approach for calculating the energetics of the real system in Table 5.

As Table 6 shows, provided a large flexible basis set is used (SBKBS2) then the three ligand models give very similar relative energies. Thus from one point of view changing the nature of the substituents from the small to the intermediate to the real system has very little effect. However we have also looked at three other ways of investigating the substituent effects at the levels of theory used for the geometry optimizations.

First, substituent effects may be studied quantitatively by comparing the relative energies for the small and intermediate structural models at identical levels of theory. We have tabulated these "substituent values"[90] in Table 7. (To evaluate the substituent value at RHF/LANL2MB we have reoptimized the small model structures at this level of theory.) The results in Table 7 show that there is quite a variation in the substituent effect at the RHF/LANL2MB level, although to some extent this is due to the use of the unconstrained ligand. The values at B3LYP/SBK show much less variation; however, they still change sign and indicate a lack of consistency in the substituent effects. Of perhaps more interest is to compare the substituent values between the RHF and B3LYP methods for each structure. Levels of theory with similar substituent values may be combined in an ONIOM calculation with greater confidence. In this case

Table 8. Component Energies (kcal mol^{-1}) for IMOMM Calculations[a]

structure	MM contribution	MO contribution	IMOMM rel E	MO destabilization[b]
1	0	0	0	15.2(10.4)
2	1.3(1.7)	45.8(30.3)	47.1(32.0)	18.1(14.2)
3	2.6(6.7)	−2.5(20.4)	0.1(27.1)	22.9(29.0)
7	−2.1(4.8)	−16.0(−12.2)	−18.1(−7.4)	13.1(13.7)

[a] Results shown are for IMOMM(RHF/LANL2MB intermediate:MM3 real) and, in parentheses, for IMOMM(B3LYP/SBK intermediate:MM3 real). [b] MO destabilization = RHF/LANL2MB component of IMOMM calculation − RHF/LANL2MB//RHF/LANL2MB energy (from level "d"), and in parentheses MO destabilization = B3LYP/SBK component of IMOMM calculation − B3LYP/SBK//B3LYP/SBK energy (from level "f").

Table 7 shows that for at least some of the structures the agreement between the levels of theory is rather poor.

Second, the effect of substituents can be further assessed by comparing a with e (Table 5), d with h, and f with i (each of these comparisons evaluates the effect of including substituents via the ONIOM method). The first of these comparisons (making use of the Zr−P constrained "a" results) shows that the substituents generally raise the relative energies by a small amount. The second comparison (d with h) shows that **2**−**8** are destabilized, while **13**, **14**, and **17** are stabilized considerably. Finally the comparison of f with i shows a consistent destabilization for most structures, but a substantial stabilization again for **13** and **17**.

Third, an analysis of the IMOMM component energies for the real system is shown in Table 8 (the relative energies for these levels of theory are shown in the Supporting Information). This shows a breakdown of the overall relative energy into contributions from the molecular orbital part and the molecular mechanics part of the IMOMM calculations. For both sets of IMOMM calculations the MO part dominates. This table also includes the "MO destabilisation energy" which is a measure of the absolute change in the MO portion of the molecule caused by the geometry distorting to accommodate the MM substituents (in this case, the $SiMe_2$ groups and the PPh group). The values for both sets of IMOMM calculations are fairly similar and indicate that the substituent destabilization is about the same for structures **1**, **2**, and **7** but somewhat larger for **3** at the B3LYP level.

Concluding Remarks

In this paper we have compared a number of different structural models and levels of theory for representing the reaction of a binuclear zirconium dinitrogen complex. First in terms of geometries, most of the structures for **1**−**17** look quite similar with the different approaches we have used. The problem of phosphine dissociation is fixed with the larger macrocyclic ligand. The phenyl groups on the phosphines, together with the macrocyclic ligand, are essential to get the correct planarity of the Zr_2N_2 portion of structures **1**, **2**, and **3**. Second in terms of energetics, our component analysis suggests that there are some moderately large effects on the absolute energies of the central region caused by the surrounding substituents. However the relative energetic effects of the substituents appear to be small (particularly

with the use of the large flexible SBKBS2 basis set), and therefore the model we used in our earlier work does indeed appear to be a good model. Some of the activation energies may be larger than we originally calculated and we have now clarified the intermediacy of structure **7** for both pathways A and B, but otherwise our original potential energy surface and mechanism are quite satisfactory.

Finally we note that the molecular orbital calculations on the intermediate model and the ONIOM calculations on the real system are still quite time-consuming, particularly when detailed exploration of potential energy surfaces and investigation of subtle conformational effects is required. The work presented here lends support to our use of simple theoretical models to represent moderately large experimental structures. It is probably more efficient, without sacrificing reliability, to mimic experimental ligands by choosing simple hydrides with constrained distances (and angles) to obtain realistic structures. Such approaches have been used successfully by us and others for a variety of recent experimental systems.[34,68]

Acknowledgment. This work was supported by the Australian Research Council, the Australian Academy of Science, and in part by a grant (CHE-0209660) from the National Science Foundation. Acknowledgment is made for generous support of computing time at the Emerson Center of Emory University, the Maui High Performance Computing Center, and the Australian Partnership for Advanced Computing. B.F.Y. acknowledges the award of an Emerson Fellowship and is grateful to Dmitry Khoroshun for patiently answering many questions. We thank the anonymous referees for helping to strengthen this manuscript.

Supporting Information Available: Comparisons of theory with experiment for structure **7**, total energies and Cartesian coordinates of all structures, details of basis sets employed, and the complete references for refs 86−88. This material is available free of charge via the Internet at http://pubs.acs.org.

References

(1) Ertl, G. In *Catalytic Ammonia Synthesis*; Jennings, J. R., Ed.; Plenum: New York, 1991.

(2) Eady, R. R. *Perspectives on Bioinorganic Chemistry*; JAI Press: Greenwich, CT, 1991.

(3) Leigh, G. J. *Acc. Chem. Res.* **1992**, *25*, 177−181.

(4) Kim, J.; Rees, D. C. *Nature* **1992**, *360*, 553.

(5) Kim, J.; Rees, D. C. *Science* **1992**, *257*, 1667.

(6) Chan, M. K.; Kim, J.; Rees, D. C. *Science* **1993**, *260*, 792.

(7) Deng, H.; Hoffmann, R. *Angew. Chem., Int. Ed. Engl.* **1993**, *32*, 1062−1065.

(8) Ludden, P. W. In *Encyclopedia of Inorganic Chemistry*; Wiley: New York, 1994; p 2566.

(9) Coucouvanis, D. In *Encyclopedia of Inorganic Chemistry*; Wiley: New York, 1994; p 2557.

(10) Demadis, K. D.; Coucouvanis, D. *Inorg. Chem.* **1995**, *34*, 436.

(11) Howard, J. B.; Rees, D. C. *Chem. Rev.* **1996**, *96*, 2983.

(12) Burgess, B. K.; Lowe, D. J. *Chem. Rev.* **1996**, *96*, 2983.

(13) Eady, R. R. *Chem. Rev.* **1996**, *96*, 3013.

(14) Malinak, S. M.; Simeonov, A. M.; Mosier, P. E.; McKenna, C. E.; Coucouvanis, D. *J. Am. Chem. Soc.* **1997**, *119*, 1662.

(15) Fryzuk, M. D.; Love, J. B.; Rettig, S. J.; Young, V. G. *Science* **1997**, *275*, 1445−1447.

(16) Ferguson, R.; Solari, E.; Floriani, C.; Osella, D.; Ravera, M.; Re, N.; Chiesi-Villa, A.; Rizzoli, C. *J. Am. Chem. Soc.* **1997**, *119*, 10104−10115.

(17) Sellmann, D.; Sutter, J. *Acc. Chem. Res.* **1997**, *30*, 460−469.

(18) Neyman, K. M.; Nasluzov, V. A.; Hahn, J.; Landis, C. R.; Rösch, N. *Organometallics* **1997**, *16*, 995−1000.

(19) Campazzi, E.; Solari, E.; Floriani, C.; Scopelliti, R. *Chem. Commun.* **1998**, 2603−2604.

(20) Leigh, G. J. *Science* **1998**, *279*, 506.

(21) Nishibayashi, Y.; Iwai, S.; Hidai, M. *Science* **1998**, *279*, 540.

(22) Fryzuk, M. D.; Love, J. B.; Rettig, S. J. *Organometallics* **1998**, *17*, 846−853.

(23) Tuczek, F.; Lehnert, N. *Angew. Chem., Int. Ed. Engl.* **1998**, *37*, 2636−2638.

(24) Basch, H.; Musaev, D. G.; Morokuma, K.; Fryzuk, M. D.; Love, J. B.; Seidel, W. W.; Albinati, A.; Koetzle, T. F.; Klooster, W. T.; Mason, S. A.; Eckert, J. *J. Am. Chem. Soc.* **1999**, *121*, 523−528.

(25) Basch, H.; Musaev, D. G.; Morokuma, K. *J. Am. Chem. Soc.* **1999**, *121*, 5754−5761.

(26) Musaev, D. G.; Cui, Q.; Svensson, M.; Morokuma, K. In *Transition State Modeling for Catalysis*; Truhlar, D. G., Morokuma, K., Eds.; American Chemical Society: Washington, DC, 1999; pp 198−207.

(27) Khoroshun, D. V.; Musaev, D. G.; Morokuma, K. *Organometallics* **1999**, *18*, 5653−5660.

(28) Lehnert, N.; Tuczek, F. *Inorg. Chem.* **1999**, *38*, 1671−1682.

(29) Ishino, H.; Tokunaga, S.; Seino, H.; Ishii, Y.; Hidai, M. *Inorg. Chem.* **1999**, *38*, 2489−2496.

(30) Clentsmith, G. K. B.; Bates, V. M. E.; Hitchcock, P. B.; Cloke, F. G. N. *J. Am. Chem. Soc.* **1999**, *121*, 10444−10445.

(31) Peters, J. C.; Cherry, J.-P. F.; Thomas, J. C.; Baraldo, L.; Mindiola, D. J.; Davis, W. M.; Cummins, C. C. *J. Am. Chem. Soc.* **1999**, *121*, 10053−10067.

(32) Mindiola, D. J.; Meyer, K.; Cherry, J.-P. F.; Baker, T. A.; Cummins, C. C. *Organometallics* **2000**, *19*, 1622−1624.

(33) Fryzuk, M. D.; Johnson, S. A. *Coord. Chem. Rev.* **2000**, *200−202*, 379−409.

(34) Basch, H.; Musaev, D. G.; Morokuma, K. *Organometallics* **2000**, *19*, 3393−3403.

(35) Caselli, A.; Solari, E.; Scopelliti, R.; Floriani, C.; Re, N.; Rizzoli, C.; Chiesi-Villa, A. *J. Am. Chem. Soc.* **2000**, *122*, 3652−3670.

(36) Dubé, T.; Ganesan, M.; Conoci, S.; Gambarotta, S.; Yap, G. P. A. *Organometallics* **2000**, *19*, 3716−3721.

(37) Guan, J.; Dubé, T.; Gambarotta, S.; Yap, G. P. A. *Organometallics* **2000**, *19*, 4820−4827.

(38) Fryzuk, M. D.; Johnson, S. A.; Patrick, B. O.; Albinati, A.; Mason, S. A.; Koetzle, T. F. *J. Am. Chem. Soc.* **2001**, *123*, 3960−3973.

(39) Solari, E.; Hesschenbrouck, J.; Scopelliti, R.; Floriani, C.; Re, N. *Angew. Chem., Int. Ed. Engl.* **2001**, *40*, 932−934.

(40) Solari, E.; Da Silva, C.; Iacono, B.; Hesschenbrouck, J.; Rizzoli, C.; Scopelliti, R.; Floriani, C. *Angew. Chem., Int. Ed. Engl.* **2001**, *40*, 3907−3909.

(41) Bielawa, H.; Hinrichsen, O.; Birkner, A.; Muhler, M. *Angew. Chem., Int. Ed. Engl.* **2001**, *40*, 1061−1063.

(42) Evans, W. J.; Allen, N. T.; Ziller, J. W. *J. Am. Chem. Soc.* **2001**, *123*, 7927−7928.

(43) Chirik, P. J.; Henling, L. M.; Bercaw, J. E. *Organometallics* **2001**, *20*, 534−544.

(44) Roussel, P.; Errington, W.; Kaltsoyannis, N.; Scott, P. *J. Organomet. Chem.* **2001**, *635*, 69−74.

(45) Greco, G. E.; Schrock, R. R. *Inorg. Chem.* **2001**, *40*, 3861−3878.

(46) Hidai, M.; Mizobe, Y. *Pure Appl. Chem.* **2001**, *73*, 261−263.

(47) Smith, J. M.; Lachicotte, R. J.; Pittard, K. A.; Cundari, T. A.; Lukat-Rodgers, G.; Rodgers, K. R.; Holland, P. L. *J. Am. Chem. Soc.* **2001**, *123*, 9222−9223.

(48) Fryzuk, M. D.; Kozak, C. M.; Bowdridge, M. R.; Patrick, B. O.; Rettig, S. J. *J. Am. Chem. Soc.* **2002**, *124*, 8389−8397.

(49) Musaev, D. G.; Basch, H.; Morokuma, K. In *Computational Modeling of Homogeneous Catalysis*; Maseras, F., Lledos, A., Eds.; Kluwer Academic Publ.: 2002; pp 325−361.

(50) Studt, F.; Morello, L.; Lehnert, N.; Fryzuk, M. D.; Tuczek, F. *Chem.--Eur. J.* **2003**, *9*, 520−530.

(51) Fryzuk, M. D.; MacKay, B. A.; Patrick, B. O. *J. Am. Chem. Soc.* **2003**, *125*, 3234−3235.

(52) Fryzuk, M. D. *Chem. Rec.* **2003**, *3*, 2−11.

(53) Shaver, M. P.; Fryzuk, M. D. *Adv. Synth. Catal.* **2003**, *345*, 1061−1076.

(54) Yandulov, D. V.; Schrock, R. R. *Science* **2003**, *301*, 76−78.

(55) Schrock, R. R. *Chem. Commun.* **2003**, 2389−2391.

(56) Studt, F.; MacKay, B. A.; Fryzuk, M. D.; Tuczek, F. *J. Am. Chem. Soc.* **2004**, *126*, 280−290.

(57) Pool, J. A.; Lobkovsky, E.; Chirik, P. J. *Nature* **2004**, *427*, 527−530.

(58) Fryzuk, M. D. *Nature* **2004**, *427*, 498−499.

(59) MacKay, B. A.; Fryzuk, M. D. *Chem. Rev.* **2004**, *104*, 385−401.

(60) Nishibayashi, Y.; Saito, M.; Uemura, S.; Takekuma, S.; Takekuma, H.; Yoshida, Z. *Nature* **2004**, *428*, 279−280.

(61) Musaev, D. G. *J. Phys. Chem. B* **2004**, *108*, 10012−10018.

(62) Evans, W. J.; Lee, D. S.; Rego, D. B.; Perotti, J. M.; Kozimor, S. A.; Moore, E. K.; Ziller, J. W. *J. Am. Chem. Soc.* **2004**, *126*, 14574−14582.

(63) Pool, J. A.; Bernskoetter, W. H.; Chirik, P. J. *J. Am. Chem. Soc.* **2004**, *126*, 14326−14327.

(64) Kozak, C. M.; Mountford, P. *Angew. Chem., Int. Ed.* **2004**, *43*, 1186−1189.

(65) Hanna, T. E.; Lobkovsky, E.; Chirik, P. J. *J. Am. Chem. Soc.* **2004**, *126*, 14688−14689.

(66) Bobadova-Parvanova, P.; Wang, Q.; Morokuma, K.; Musaev, D. G. *Angew. Chem., Int. Ed. Engl.* **2005**, *44*, 7101−7103.

(67) Blomberg, M. R. A.; Siegbahn, P. E. M. *J. Am. Chem. Soc.* **1993**, *115*, 6908−6915.

(68) Fryzuk, M. D.; Johnson, S. A.; Rettig, S. J. *Organometallics* **2000**, *19*, 3931−3941.

(69) Froese, R. D. J.; Morokuma, K. In *The Encyclopedia of Computational Chemistry*; Schleyer, P. v. R., Allinger, N. L., Clark, T., Gasteiger, J., Kollman, P. A., Schaefer, H. F., III, Schreiner, P. R., Eds.; John Wiley: Chichester, 1998; pp 1245−1257.

(70) Dapprich, S.; Komaroni, I.; Byun, K. S.; Morokuma, K.; Frisch, M. J. *J. Mol. Struct. (THEOCHEM)* **1999**, *461−462*, 1−21.

(71) Hay, P. J.; Wadt, W. R. *J. Chem. Phys.* **1985**, *82*, 299−310.

(72) Stevens, W. J.; Basch, H.; Krauss, M. *J. Chem. Phys.* **1984**, *81*, 6026.

(73) Stevens, W. J.; Krauss, M.; Basch, H.; Jasien, P. G. *Can. J. Chem.* **1992**, *70*, 612.

(74) Becke, A. D. *J. Chem. Phys.* **1993**, *98*, 5648.

(75) Lee, C.; Yang, W.; Parr, R. G. *Phys. Rev. B* **1988**, *37*, 785−789.

(76) Stephens, P. J.; Devlin, J. F.; Chabalowski, C. F.; Frisch, M. J. *J. Phys. Chem.* **1994**, *98*, 11623−11627.

(77) Seeger, R.; Pople, J. A. *J. Chem. Phys.* **1977**, *66*, 3045−3050.

(78) Bauernschmitt, R.; Ahlrichs, R. *J. Chem. Phys.* **1996**, *104*, 9047−9052.

(79) Maseras, F.; Morokuma, K. *J. Comput. Chem.* **1995**, *16*, 1170−1179.

(80) Matsubara, T.; Maseras, F.; Koga, N.; Morokuma, K. *J. Phys. Chem.* **1996**, *100*, 2573.

(81) Matsubara, T.; Sieber, S.; Morokuma, K. *Int. J. Quantum Chem.* **1996**, *60*, 1101−1109.

(82) Maseras, F.; Lledos, A.; Clot, E.; et al. *Chem. Rev.* **2000**, *100*, 601−636.

(83) Rappé, A. K.; Casewit, C. J.; Colwell, K. S.; Goddard, W. A.; Skiff, W. M. *J. Am. Chem. Soc.* **1992**, *114*, 10024−10035.

(84) Allinger, N. L. *MM3(92)*; Quantum Chemistry Program Exchange: Indiana University, 1992.

(85) Aped, A.; Allinger, N. L. *J. Am. Chem. Soc.* **1992**, *114*, 4.

(86) Frisch, M. J. et al. *Gaussian 98 A.1, Revision A.1*; Gaussian, Inc.: Pittsburgh, PA, 1998.

(87) Frisch, M. J. et al. *Gaussian 03, Revision B.03*; Gaussian, Inc.: Pittsburgh, PA, 2003.

(88) Frisch, M. J. et al. *Gaussian 92/DFT, Revision F*; Gaussian, Inc.: Pittsburgh, PA, 1993.

(89) Deeth, R. *J. Organomet. Chem.* **2001**, *635*, 165−172.

(90) Morokuma, K.; Musaev, D. G.; Vreven, T.; Basch, H.; Torrent, M.; Khoroshun, D. V. *IBM J. Res. Dev.* **2001**, *45*, 367−395.

CT050320E